

Fabrication of Highly Interconnected Poly(ϵ -caprolactone)/cellulose Nanofiber Composite Foams by Microcellular Foaming and Leaching Processes

Jiawei Li, Hongyao Wang, Hongfu Zhou,* Jing Jiang,* Xiaofeng Wang, and Qian Li

Cite This: *ACS Omega* 2021, 6, 22672–22680

Read Online

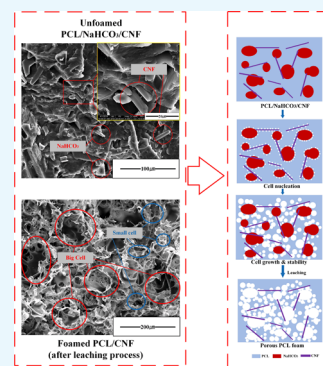
ACCESS |

Metrics & More

Article Recommendations

Supporting Information

ABSTRACT: In this study, microcellular polycaprolactone (PCL)/sodium bicarbonate (NaHCO_3)/cellulose nanofiber (CNF) composite foams with highly interconnected porous structures were successfully fabricated by microcellular foaming and particle leaching processes. Supercritical CO_2 (scCO_2) served as a physical foaming agent, NaHCO_3 was chosen as a chemical foaming agent and porogen, and CNF acted as a heterogeneous nucleating agent. The effect of scCO_2 , NaHCO_3 , and CNF on pore structures and the cofoaming mechanism were investigated. The results indicated that the addition of NaHCO_3 and CNF increased the melt strength of the PCL matrix significantly. During the foaming process, the presence of CNF can form a rigid network due to the hydrogen bonding or mechanical entanglement between individual nanofibers, improving the nucleating efficiency but slowing down the cell growth rate. Additionally, due to the interaction of “soft” PCL matrix and “hard” domains in a PCL-based composite during the foaming process, together with the NaHCO_3 leaching process, highly interconnected cell structures appeared. The obtained PCL/ NaHCO_3 /CNF composite foams had a cell size of 15.8 μm and cell density of 6.3×10^7 cells/ cm^3 , as well as an open-cell content of 82%. The reported strategy in this paper may provide the guidelines and data supports for the fabrication of a PCL-based porous scaffold.



INTRODUCTION

The study of biodegradable recycled plastics is the development trend of green sustainable materials. With its unique interconnectivity and a three-dimensional (3D) skeleton structure, open-cell polymer foam materials are widely used in sound-absorbing materials, petroleum absorbent materials, wastewater or sewage treatment materials, optical materials, biomedical materials, conductive materials, and filter membrane materials.¹ Nanocomposite foams provide new opportunities to produce tissue engineering, cancer treatment, medical imaging, dental applications, drug delivery, and other modern medicine products.^{2,3}

In recent years, the preparation of a porous scaffold has attracted the attention of many researchers.⁴ An ideal porous scaffold should have adequate cell size and distribution, with high porosity and high connectivity between cells.⁵ Several methods have been used to prepare porous scaffolds commonly, such as thermally induced phase separation, solution casting, particle leaching, electrospinning, and gas foaming. Among them, the open-cell material prepared by thermally induced phase separation is easy to retain organic solvents, and the solvent recovery cost is expensive. The pore diameter of the polymer open-pore materials prepared by the thermal decomposition method is more affected by thermally unstable parts. The electrospinning method is limited by the phase structure of the blend and uses organic solvents. The preparation methods of these open-pored microporous

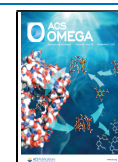
materials require high material selection or process parameter control and are not suitable for large-scale production and application.

Until now, various technologies (e.g., phase separation, solvent extraction, electrospinning, 3D printing, and gas foaming^{6–9}) have been reported based on biodegradable polymers to prepare porous structures. Supercritical gas foaming is attracting increasing interest because of its advantages of being solvent-free and ecofriendly.¹⁰ In this process, CO_2 is widely used as a physical blowing agent due to the high dissolution in polymer, nontoxicity, and low cost.^{11,12} By increasing the temperature or decreasing the pressure, the saturated gas's solubility in the polymer–gas homogeneous system will fall, and the gas will escape and cause bubble nucleation. Since the nucleation barrier at the interface is lower than the homogeneous system inside the polymer, the bubble nucleus is preferentially formed at the two-phase interface. For incompatible polymer systems, the binding effect between the two-phase interface is weak. Cell growth will cause the two-phase interface to separate from each other, forming an open-

Received: May 26, 2021

Accepted: August 12, 2021

Published: August 25, 2021



pore structure with interconnected pores.¹³ Polymer nanocomposites are described as polymers that contain fillers lower than 100 nm in at least one dimension¹⁴—usually adding nanodimensional fillers to the polymer, PLA,¹⁵ TPU,¹⁶ and PA.¹⁷

In most cases, low interconnectivity results are obtained based on scCO₂ foaming because the gas expansion force is too small to overcome the strength of the polymer matrix.¹⁸ Particle leaching is an effective process for fabricating highly interconnected porous structures. This technique blends water-soluble inorganic particles with one matrix material. The disadvantages of unpredictable pore sizes and poor mechanical properties have been detected by a single-particle leaching process. To further improve the open-cell content of the porous materials, mixed processes combining gas foaming and particle leaching can be used and are attracting increasing attention^{19,20}

Polycaprolactone (PCL) has attracted increasing interest in biomedical fields, such as tissue engineering, drug delivery, absorbable sutures, and implant materials²¹ as a promising synthetic biodegradable and biocompatible polymer.²² A cellulose nanofiber (CNFs) is a unique and abundant renewable resource commonly found in plants and animals. It has a high specific surface area, low density, and high mechanical strength.²³ CNFs have a short length, without any particle entanglement, and possess a high Young's modulus (between 130 and 250 GPa).²⁴ Therefore, cellulose nanocrystals (CNCs) are promising materials that have the potential to be used in many applications such as reinforcement agents in polymer nanocomposites.

In this paper, CO₂ and NaHCO₃ served as coblowing agents. Microcellular batch foaming and particle leaching processes were combined to fabricate PCL/NaHCO₃/CNF composite open foams. Thermal and rheological behaviors of PCL-based composites were studied first to evaluate the crystallization properties and foaming feasibility, respectively. The effect of dispersed NaHCO₃ and CNF on the morphology of composites was then investigated. Meanwhile, we explored the impact of CNF dispersion and NaHCO₃ leaching on PCL foaming behaviors. Cell size, cell density, cell uniformity, volume expansion ratio, and cell-open content were measured qualitatively and quantitatively. Finally, the cofoaming mechanism was also discussed.

MATERIALS AND METHODS

Materials. A semicrystalline poly(ϵ -caprolactone) (PCL, CAPA 6500 from Perstorp, U.K.) was used as a matrix polymer. The molecular weight $M_n = 50\,000$ g/mol. It had a density of 1.14 g/cm³ and the melt point was 58 °C. Sodium bicarbonate (NaHCO₃, Alkali Industry Development Co., Ltd., China) with a density 2.159 g/cm³ was applied as a porogen and a chemical foaming agent, which could be partly decomposed to CO₂ and water vapor at temperatures above 50 °C²⁵ (especially under supercritical conditions).

Acetylated cellulose nanofibers (CNFs) were prepared from Nakaratesco, Kyoto, Japan (Supporting Information S1). The existence of hydroxyl groups makes the CNFs' surface activity higher. Compared with native CNFs, the hydrophobic modification for CNFs is efficient for improving the dispersibility in a polymer matrix.²⁶ The characteristic data of acetylated CNFs are given in Table 1. The morphology of CNF powders is shown in Figure 1.

Table 1. Characteristics of CNFs

cellulose content (%)	degree of substitution (%)	degree of oxidation (%)	ζ -potential (mv)	carboxylic groups content (mmol/g)
92	60	97	-15	2.4

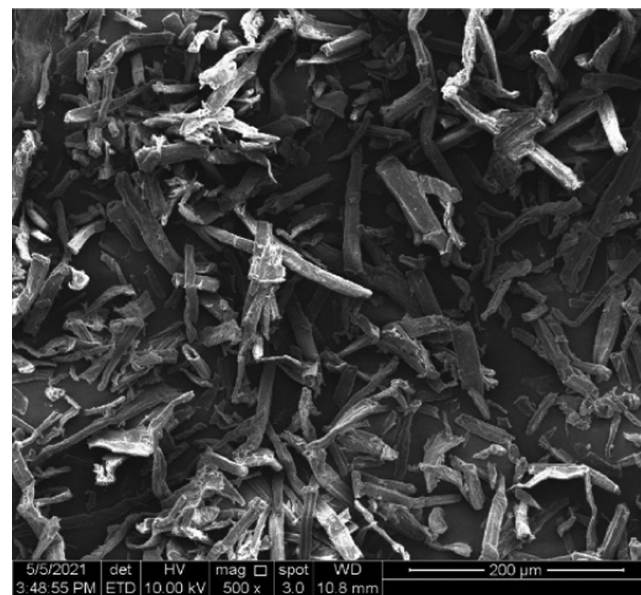


Figure 1. Micrograph of CNFs.

CO₂ with a purity of 99.9% (JiningXieli Special Gas Co, Ltd., China) was used as a physical foaming agent for the microcellular batch foaming process. Dichloromethane (DCM) was supplied by Tianjin Kemiou Chemical Co., Ltd. (Tianjin, China).

Sample Preparation. A solution blending process was used in this experiment so that NaHCO₃ and CNFs powders can achieve good dispersity in a PCL matrix. The neat PCL and raw CNF materials were first dried for 12 h at 30 °C in a vacuum oven. PCL was dissolved into a DCM at a concentration of 10% (w/v). NaHCO₃ and CNF were then added to the solution, in turn, which was subjected to ultrasonic oscillations for 10 min to ensure that NaHCO₃ and CNF were well distributed in the solution. Finally, the colloid was poured into a circular holder made of polytetrafluoroethylene and air-dried for 24 h to prepare a film with a thickness of 350–400 μ m. The PCL composites formulations are given in Table 2.

A homemade supercritical foaming device was used in the foaming process. The comparison flow chart is shown in Figure 2. The system includes an autoclave for sterilization (SLM-D, Beijing Century Senlang Test Instrument Co., Ltd., China) and a heating tool for heating the autoclave high-pressure

Table 2. Composition Ratio of PCL/NaHCO₃/CNF Composites (by Weight)

materials	weight ratio (%)		
	A: neat PCL	B: PCL/NaHCO ₃	C: PCL/NaHCO ₃ /CNF
PCL	100	70	69
NaHCO ₃	0	30	30
CNF	0	0	1 ^a

^aSupporting Information S2.

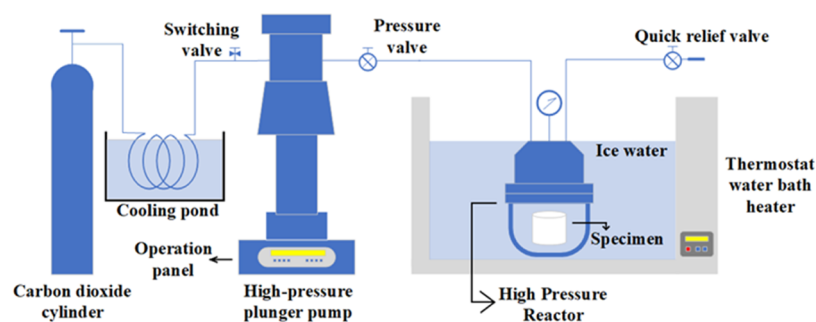


Figure 2. Schematic diagram of the supercritical foaming equipment.

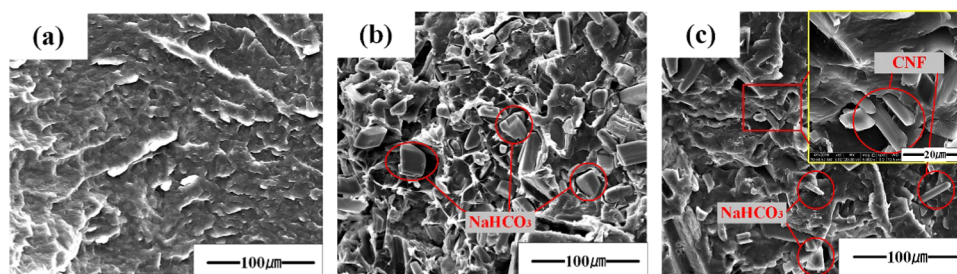


Figure 3. Morphologies of PCL-based composites: (a) neat PCL, (b) PCL/NaHCO₃, and (c) PCL/NaHCO₃/CNF.

plunger pump (ISCO-D, Worldwide Innovation Co, Ltd.). The gas was extracted from the carbon dioxide cylinder and injected into the autoclave. To increase the open-cell content and interconnection of the foamed scaffolds, we leached out the NaHCO₃ phase by a circulating water bath. The whole process lasted about 24 h to remove all of the NaHCO₃ and Na₂CO₃. In the end, all of the samples were dried in the oven and collected for later use.

CHARACTERIZATION

Differential Scanning Calorimetry (DSC). The composite samples were characterized by a TA Q20 machine. The samples were heated to 100 °C first at a heating rate of 10 °C/min under a nitrogen atmosphere and held for 5 min to eliminate the thermal history. The samples were then cooled to 0 °C at a cooling rate of 10 °C/min and then heated to 100 °C again to record melting and crystallization behaviors.

The relative crystallinity (X_c) of PCL was calculated by the formula 1 as follows

$$X_c = \frac{\Delta H_f}{X^* \cdot \Delta H_m} \times 100\% \quad (1)$$

where ΔH_f is the melting enthalpy of PCL, X^* is the weight fraction of PCL material in composites, ΔH_m is the melting heat enthalpy of 100% crystalline, and PCL is 139 J/g.²⁰

Rheology. Linear dynamic rheological measurements were performed on all samples by a rotational rheometer (DHR-2, TA) with a parallel plate geometry ($\phi 25$ mm) with a gap of 1 mm. The strain sweep scan was pretested to find a suitable strain range to ensure that all tests were conducted in the linear viscoelastic region. The dynamic frequency sweep mode was then carried out with a temperature of 100 °C, 1.0% strain, and frequency within 0.01–100 rad/s under gaseous nitrogen flow to avoid thermal-oxidative degradation.

Scanning Electron Microscopy (SEM). All foamed samples were immersed into the liquid nitrogen and then fractured. The cross section was sprayed with a thin platinum

layer using an ion sputtering apparatus (SC7620, Quorum Technologies). The final processed section was characterized by scanning electron microscopy (SEM, JSM-6060, JEOL). The average cell size and cell density in SEM micrographs were measured by Image J. Pro.

The cell density (N_f) of the foamed sample can be calculated by the formula

$$N_f = \frac{N^{3/2}}{A} \quad (2)$$

where N is the number of bubbles in the microscope photo and A is the area of the selected microscope photo (unit: cm²).

The volume expansion ratio (VER) was measured by the water displacement method and the formula is shown as 3

$$VER = \frac{\rho_{\text{solid}}}{\rho_{\text{foam}}} \quad (3)$$

where ρ_{solid} is the density of solid materials and ρ_{foam} is the density of foamed materials.

Open-Cell Content. The open-cell content (OCC) was obtained from eq 4 as follows

$$OCC = \frac{v_{\text{cell}}}{v_{\text{polymer}}} \times 100\% \quad (4)$$

where v_{cell} is the open-cell volume, which can be obtained using a helium pycnometer (ULTRAPYC 1200e, Quanta chrome Instruments), while v_{polymer} is the total volume of the polymer.

RESULTS AND DISCUSSION

Phase Morphologies. The dispersion of NaHCO₃ and CNF in the PCL matrix has a big influence on PCL's cell nucleation during the microcellular process. The phase morphologies of PCL-based composites were first compared in Figure 3. As shown in Figure 3a, the neat PCL formed a relatively flat ductile section, while there was a distinct stripping phenomenon in the PCL matrix shown in Figure

3b, which can be attributed to NaHCO_3 's lamellar structure. The physical cross-linking point would be reduced because of the aggregation of inorganic particles in the PCL matrix. It can be seen from Figure 3c that no apparent voids were observed, which demonstrates that the interface bonding force between the PCL matrix and the dispersed CNF was high. In other words, the CNFs were much easier to be cut off instead of being pulled out of the PCL matrix due to the reinforcement effect of the CNFs on PCL, which originates from the internal hydrogen bond interaction of CNF.²¹ Meanwhile, it is well known that homogeneous dispersion of CNFs is efficient for uniform foam structures.²⁷ Since the diameter of CNF used in this experiment was on the micron scale, much smaller risk of agglomeration behaviors happened compared to that of nanofibers. The dispersity of CNF in the PCL matrix can also be improved by surface chemical modification because the existence of a large number of hydroxyl groups on the surface of CNF gives it high surface activity.

Crystallization Behaviors. To evaluate PCL composites' influence on the thermal properties, DSC was conducted to measure the crystallization behaviors for all samples. Normally, CNF can only affect the crystallization behavior of PCL/ NaHCO_3 composites without changing or showing new crystal structures (Supporting Information S3). As is seen in Figure 4

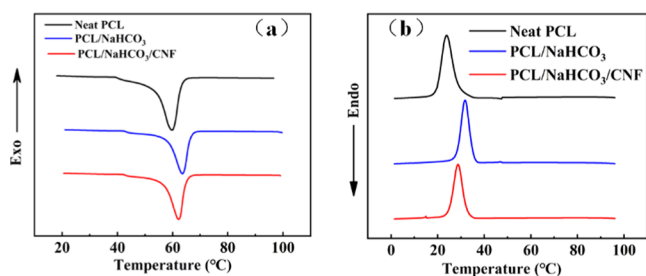


Figure 4. (a) Melting curves of PCL/ NaHCO_3 /CNF composites and (b) crystallinity curves of PCL/ NaHCO_3 /CNF composites.

Table 3. DSC Results of PCL/ NaHCO_3 /CNF Composites

sample	T_m (°C)	T_c (°C)	ΔH_m (J/g)	X_c (%)
neat PCL	60.58	23.87	83.07	59.71
PCL/ NaHCO_3	62.57	31.74	47.39	51.19
PCL/ NaHCO_3 /CNF	62.28	28.77	59.14	63.82

and Table 3, the change in melting temperature (T_m) with the addition of NaHCO_3 and CNF particles was increased. Moreover, the degree of crystallinity (X_c) and crystallinity

temperature (T_c) of neat PCL was higher than that of PCL-based composites. This reduction could be the competition result of two opposite effects of dispersed phases (NaHCO_3 and CNF) on PCL matrix crystallization. First, the presence of both NaHCO_3 and CNFs fillers improves the PCL crystallization by acting as nucleating agents.²⁸ Second, the incorporation of NaHCO_3 and CNFs into the PCL matrix restricts the movement of the PCL molecular chains.²² It is true that the hydroxyl groups of CNFs and the carbonyl groups of PCL form strong intermolecular hydrogen bonding, leading to restraining of the crystallization of PCL.²⁹ So, the decrease in X_c of the PCL composites compared to that of the neat PCL is due to the overcoming of the latter effect (movement restriction of PCL molecular chains) to that of the former (heterogeneous nucleation effect). On contrary, after adding CNFs to PCL/ NaHCO_3 composites, the CNFs still can play the role of a nucleation agent and, therefore, enhance the improvement in X_c slightly again.

Rheological Performances. Melt viscosity is considered an essential factor affecting the cell nucleation rate and cell nuclei growth during the microcellular process.³⁰ The relationship between complex viscosity of all PCL composites and the shear rate is displayed in Figure 5a. In the whole shear rate region, all samples showed shear-thinning behaviors. However, neat PCL exhibited a broader area of the Newtonian flow region than other PCL-based composites. In addition, the complex viscosities of PCL composites were higher than that of neat PCL as the result of the physical cross-linking effect from the dispersed particles (NaHCO_3 and CNF) in the PCL matrix.^{13,31} Figure 5b depicts the relationship of the samples' storage modulus as functions of the shear rate. All curves exhibited a similar trend that is the storage modulus increased with increasing shear rate. As expected, the PCL/ NaHCO_3 /CNF composite's storage modulus was remarkably higher than that of PCL/ NaHCO_3 and became less frequency-dependent at low frequencies. This less frequency dependence phenomenon indicates a gradual change from pseudoplastic-like to pseudo-solid-like behavior, reflecting the reinforcement effect of CNFs on the PCL matrix.²⁷ It seems that the CNF fillers tend to limit the long-distance movement of the matrix polymer chains and prevent them from fully relaxing when subjected to shear. Figure 5c shows the $\tan \delta$ as a function of frequency for PCL-based composites. It is found that the addition of NaHCO_3 and CNFs leads to a significant decrease in $\tan \delta$, and the dependences of $\tan \delta$ on frequency became a little bit weaker. For the sample PCL/ NaHCO_3 /CNFs, $\tan \delta$ was frequency-independent at low frequencies, and it was in a low magnitude and positive gradient with increasing frequency. This indicated that the reinforcement effect of CNFs could be

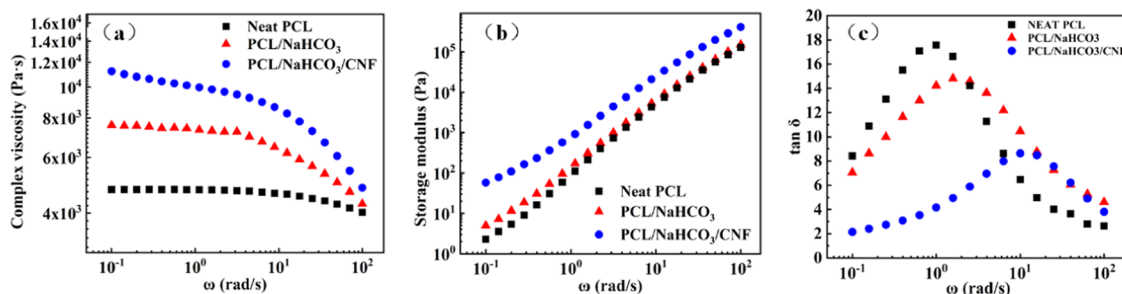


Figure 5. Rheological results of PCL/ NaHCO_3 /CNF composites: (a) complex viscosity curve, (b) storage modulus curve, and (c) $\tan \delta$ curve.

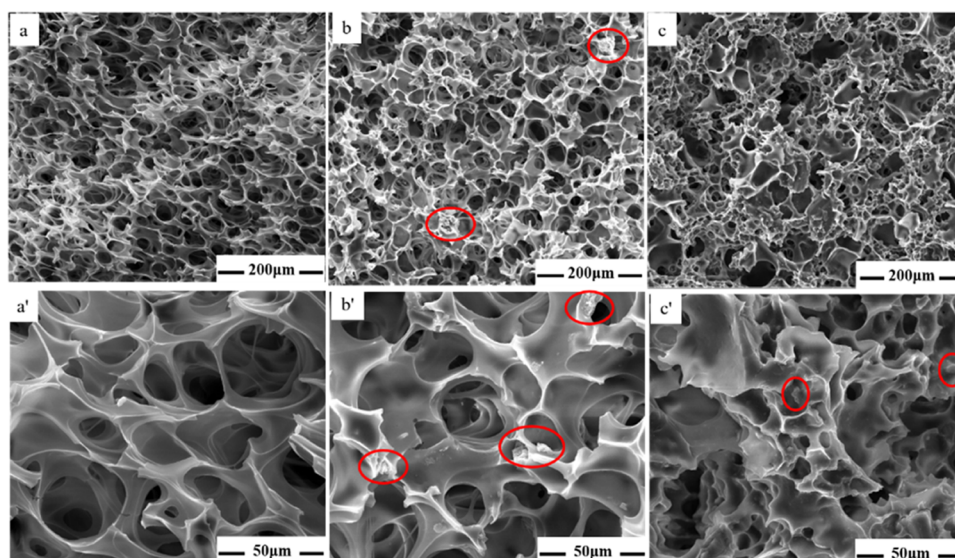


Figure 6. Pore morphologies of foamed samples before leaching NaHCO₃: (a) neat PCL, (b) PCL/NaHCO₃, and (c) PCL/NaHCO₃/CNF; (a')–(c') are enlarged images.

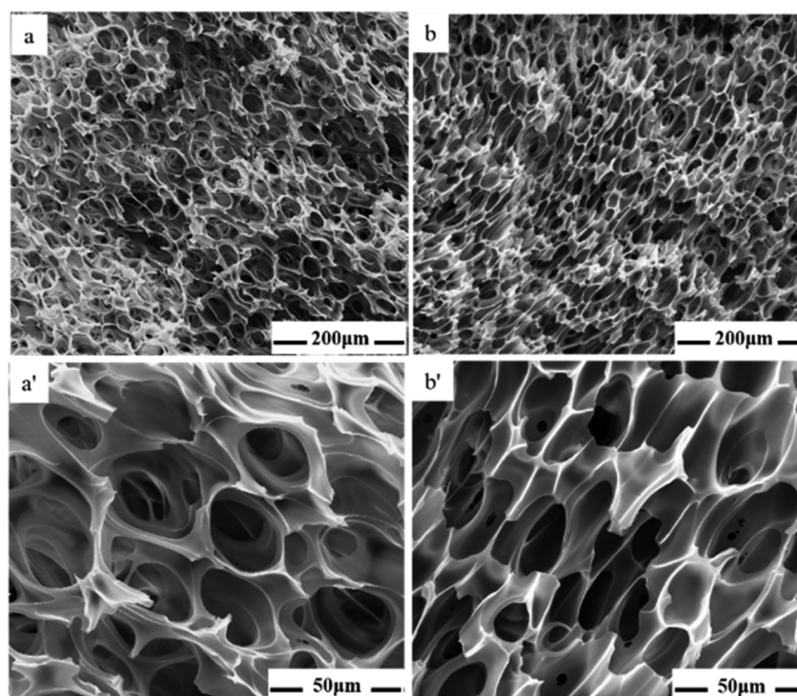


Figure 7. Pore morphologies of PCL/NaHCO₃/CNF foamed samples after leaching: (a) PCL/NaHCO₃ and (b) PCL/NaHCO₃/CNF; (a', b') enlarged images.

formed and led to the viscoelastic response behavior, changing from a liquid-like state to a solid-like state.³² The improved viscoelastic properties of PCL composites were confirmed to promote foamability during the foaming process.³³

Microcellular Foaming Properties. The presence of CNF in the nanocomposite matrix normally can accelerate the nucleation process.³⁴ The introduction of CNF into the PCL matrix significantly increased cell density and reduced cell size. This was due to the interaction between the CNF surface's nucleation and the effect of polymer rheology on cell growth.³⁵ Figure 6 shows the effect of NaHCO₃ particles and CNF on the foamed cell structure and the morphology of PCL composites before the leaching process. The foaming

conditions were as follows: saturation temperature of 50 °C, saturation pressure of 2000 PSI, and a saturation time of 1 h. Compared with the pure PCL cell morphology (Figure 6a), the addition of NaHCO₃ particles (Figure 6b,b') significantly reduces cell size and increases cell density. It is attributed to the heterogeneous nucleation effect that occurred at the interface between the PCL and NaHCO₃ interface.³⁶

In addition, compared with foamed neat PCL, nonuniform cell distribution, increased cell wall thickness, and more unfoamed regions were also found in Figure 6b. Many NaHCO₃ particles could be detected on the surface of the cell wall (red circles). After CNF fillers were added (Figure 6c), bimodal-like cell structures were found. Nonuniform cell

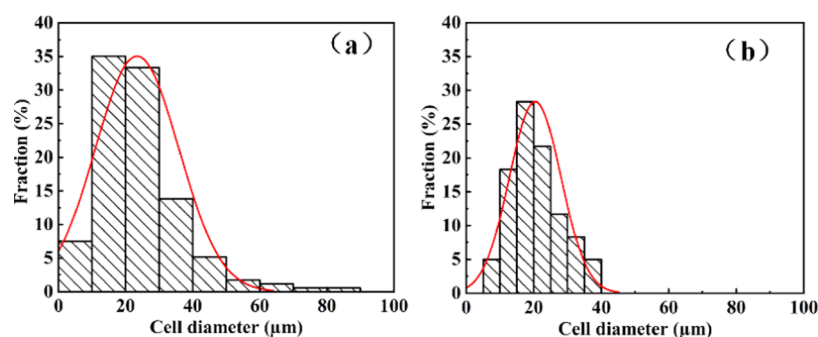


Figure 8. Pore size distribution of PCL/NaHCO₃/CNF foam samples: (a) before leaching and (b) after leaching.

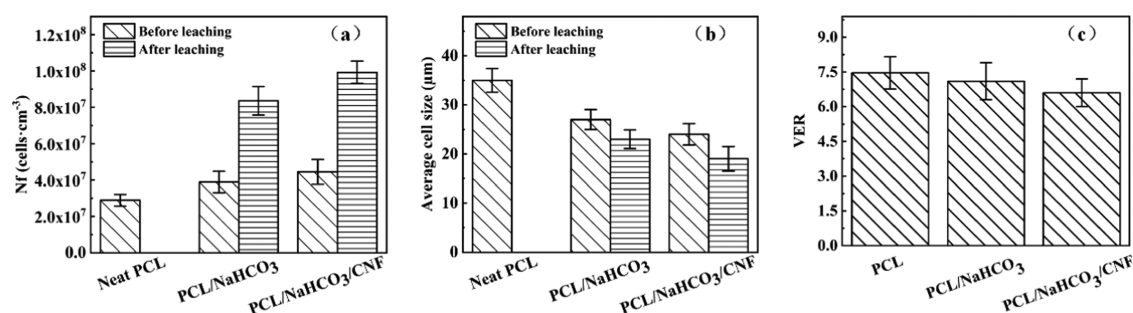


Figure 9. Cell density (a), average pore size (b), and expansion ratio (c) of PCL/NaHCO₃/CNF foam samples.

distribution appeared because of the enhanced heterogeneous nucleation effect. Both NaHCO₃ particles and CNF fillers can act as heterogeneous nucleation points during PCL foaming. Meanwhile, the melt strength of the PCL matrix could be improved after NaHCO₃ particles were added, which is efficient for PCL foaming.³⁶ It is interesting that more unfoamed regions can also be seen from Figure 6c' compared to Figure 6b'. This may be explained from the crystallinity point of view. The relative PCL crystallinity was increased obviously after adding CNF fillers compared with PCL/NaHCO₃ composites (Figure 4b), which normally can hinder the cell nucleation and growth.³⁷

Figure 7 exhibits the morphologies of foamed PCL-based composites after leaching NaHCO₃ particles. Both samples showed a highly interconnected cell structure with holes fractured in the cell walls. Fully random polygon cell shapes were also found. Foamed PCL/NaHCO₃ composites (Figure 7a,a') showed that cells were interconnected with obvious fibrillated structures at the submicron-/nanoscale connected cell walls. It was because the cell walls of the PCL matrix were stretched to a certain extent during cell growth, resulting in the decreased cell wall thickness under the function of scCO₂-induced plasticization. The matrix PCL became too weak to sustain the cell growth, leading to the bursting of the cell. Such fibrillated structures have been confirmed useful for enhancing cell adhesion and migration in the tissue engineering field.³⁸ Another interesting result from Figure 7b,b' is that many oriented cells with high interconnection appeared. This may be explained by the fact that CNF with a high aspect ratio induced cell nucleation and growth along a certain orientation.^{39,40}

Figure 8 shows the cell size distribution curves for PCL/NaHCO₃/CNF foam samples before and after the leaching process. The cell size distribution range was wider before the leaching process, and the average cell size after leaching reached 20 μm. To characterize the cell structure quantitatively, the statistical cell size, cell density, and expansion ratio

are shown in Figure 9. The average size of neat PCL was 36 μm, and the cell density was 2.0×10^7 cells/cm³. For PCL/NaHCO₃ composites, the cell density increased to 2.6×10^7 cells/cm³ and the average cell size decreased to 28 μm. After 1.0 wt % CNF was added, the cell density increased to 5.6×10^7 cells/cm³ accordingly, while the average cell size decreased to 19 μm significantly. These results were obtained because the heterogeneous nucleation effect was enhanced after NaHCO₃ and CNF were added, which increased the number of nucleation points and restricted the cell expansion.⁴¹ It was also found that there was only a slight change in the expansion ratio and the whole range was between 6.5 and 7.5 times, and the overall decline is depicted in Figure 9c. This might be related to the difficulty of processing after introducing CNF—the CNF might have shaped a 3-D network structure, as demonstrated from the high viscosity at low frequencies. The composites might have driven to small pressure drop variations when the fiber network was subjected to a quick pressure drop.¹⁵ Therefore, the addition of CNF might have had a negative effect on cell growth.

Open-Cell Content (OCC) of Foamed Composites after the Leaching Process. It is believed that the high interconnectivity of a porous scaffold may facilitate cell adhesion, proliferation, and material exchange in the tissue engineering field.⁴² The results of the open-cell content for foamed samples are shown in Figure 10. It is found that each component's open-cell content before leaching was less than 80%. The high interconnectivity of pores comes basically from the mixing of immiscible polymers.⁴³ Matrix PCL is regarded as a soft polymer, whereas scattered NaHCO₃ particles and CNF fibers are tough domains due to the high melting strength. Matrix PCL and NaHCO₃/CNF interfaces typically have lower actuation vitality boundaries and higher gas concentrations, resulting in the nucleation at the interface preferentially in the process of foaming depressurization. After the leaching process, the average increment in the open-cell content was about 8 and

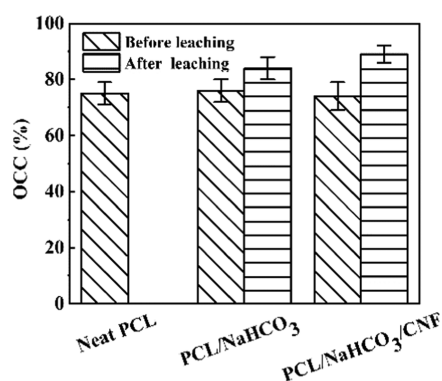


Figure 10. Open-cell content of PCL/NaHCO₃/CNF composite foams before and after leaching.

14% for foamed PCL/NaHCO₃ and PCL/NaHCO₃/CNF, respectively. This result indicated that the leaching process can help to improve the interconnectivity of cells efficiently, and contributes more open-cell content of the porous composite materials than a neat polymer.

The cell-opening mechanism is illustrated in Figure 11. Due to the different shrinkage rates of the soft PCL and NaHCO₃/CNF domains occurred during rapid cell growth, the matrix PCL with a higher shrinkage rate goes through continuous debonding from the tough NaHCO₃/CNF phase, resulting in pore opening. In other words, the bubble nucleus was formed at the phase interface because it was an incompatible polymer system; the interaction between the two-phase interfaces was fragile. The bubbles' subsequent growth would cause the polymer's adhesion to break away, thereby connecting the micropores, forming an open-cell structure. In addition, inorganic particles (NaHCO₃) and CNF also played a role in heterogeneous nucleation.

CONCLUSIONS

Highly interconnected porous PCL/NaHCO₃/CNF foams were fabricated by combining ecofriendly SCF batch foaming and particle leaching. The foaming behavior, thermal properties, rheology, and crystallization behavior of the solid samples were evaluated. The composites showed higher complex viscosity and higher crystallinity due to the reinforcement effect of CNF. The addition of NaHCO₃ and CNF increased the melt strength of the PCL matrix significantly. During the foaming process, NaHCO₃, as a heterogeneous nucleating agent, a chemical blowing agent, and a porogen, provides more CO₂ for cell growth and nucleation. The presence of CNF can form a rigid network due to the hydrogen bonding or mechanical entanglement between individual nanofibers, improving the nucleation efficiency but slowing down the

cell growth rate. Moreover, a bimodal cell structure was found after the leaching process. Small PCL foams (15–36 μm) are generated from the mixed homogeneous and heterogeneous nucleation effect, while big cells (80–150 μm) come from the thermal decomposition of NaHCO₃. The cofoaming mechanism, which consisted of NaHCO₃ leaching and “hard” NaHCO₃/CNF domains deboned from the “soft” PCL matrix, contributes to obtaining the high open-cell content of foamed composites (>80%).

ASSOCIATED CONTENT

Supporting Information

The Supporting Information is available free of charge at <https://pubs.acs.org/doi/10.1021/acsomega.1c02768>.

Chemical modification process for CNF (S1), the effect of CNF contents on pore structures (S2), and XRD results of PCL-based composites (S3) (PDF)

AUTHOR INFORMATION

Corresponding Authors

Hongfu Zhou – Beijing Key Laboratory of Quality Evaluation Technology for Hygiene and Safety of Plastics, Beijing Technology and Business University, Beijing 100048, China; orcid.org/0000-0002-9154-1798; Email: zhouhongfu@th.btbu.edu.cn

Jing Jiang – School of Mechanical & Power Engineering, Zhengzhou University, Zhengzhou 450001, China; Phone: +86 156 1796 0455; Email: jiangjing@zzu.edu.cn

Authors

Jiawei Li – School of Mechanics & Safety Engineering, National Center for International Joint research of Micro-Nano Molding Technology, Zhengzhou University, Zhengzhou 450001, China; orcid.org/0000-0002-5702-8202

Hongyao Wang – School of Mechanics & Safety Engineering, National Center for International Joint research of Micro-Nano Molding Technology, Zhengzhou University, Zhengzhou 450001, China

Xiaofeng Wang – School of Mechanics & Safety Engineering, National Center for International Joint research of Micro-Nano Molding Technology, Zhengzhou University, Zhengzhou 450001, China; orcid.org/0000-0002-8916-5404

Qian Li – School of Mechanics & Safety Engineering, National Center for International Joint research of Micro-Nano Molding Technology, Zhengzhou University, Zhengzhou 450001, China

Complete contact information is available at: <https://pubs.acs.org/doi/10.1021/acsomega.1c02768>

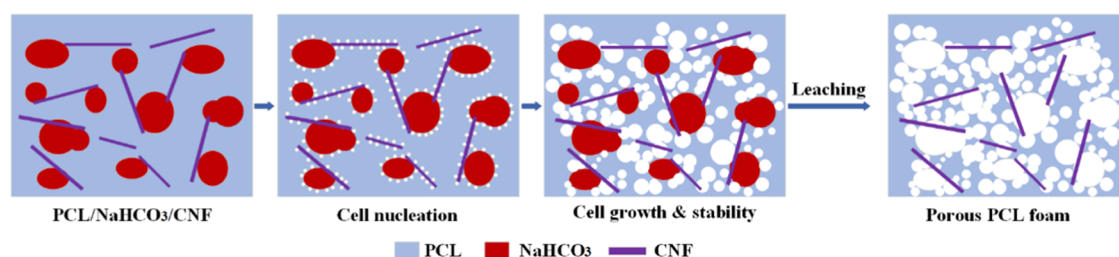


Figure 11. Schematic diagram of the cell growth for PCL/NaHCO₃/CNF composite foams.

Author Contributions

All authors participated in the preparation of this manuscript and approved the final version.

Notes

The authors declare no competing financial interest.

ACKNOWLEDGMENTS

The author would like to thank the Scientific and Technological Research Project of Henan Province (202102210028), the NSFC-Zhejiang Joint Fund for the Integration of Industrialization and Informatization (U1909219), and the research fund supported by the Key Laboratory of Processing and Quality Evaluation Technology of Green Plastics of China National Light Industry Council (PQETGP2020017).

REFERENCES

- (1) Warner, H. J.; Wagner, W. D. Fabrication of biodegradable foams for deep tissue negative pressure treatments. *J. Biomed. Mater. Res., Part B* **2018**, *106*, 1998–2007.
- (2) Di Maio, E.; Kiran, E. Foaming of polymers with supercritical fluids and perspectives on the current knowledge gaps and challenges. *J. Supercrit. Fluids* **2018**, *134*, 157–166.
- (3) Saucieu, M.; Fages, J.; Common, A.; Nikitine, C.; Rodier, E. New challenges in polymer foaming: A review of extrusion processes assisted by supercritical carbon dioxide. *Prog. Polym. Sci.* **2011**, *36*, 749–766.
- (4) Zhao, P.; Gu, H.; Mi, H.; Rao, C.; Fu, J.; Turng, L. S. Fabrication of scaffolds in tissue engineering: A review. *Front. Mech. Eng.* **2018**, *13*, 107–119.
- (5) Ahmed, A. R.; Gauntlett, O. C.; Camci-Unal, G. Origami-Inspired Approaches for Biomedical Applications. *ACS Omega* **2021**, *6*, 46–54.
- (6) Chauvet, M.; Saucieu, M.; Baillon, F.; Fages, J. Mastering the structure of PLA foams made with extrusion assisted by supercritical CO₂. *J. Appl. Polym. Sci.* **2017**, *134*, No. 45067.
- (7) Nofar, M.; Park, C. B. Poly (lactic acid) foaming. *Prog. Polym. Sci.* **2014**, *39*, 1721–1741.
- (8) Ding, W.; Jahani, D.; Chang, E.; Alemdar, A.; Park, C. B.; Sain, M. Development of PLA/cellulosic fiber composite foams using injection molding: Crystallization and foaming behaviors. *Composites, Part A* **2016**, *83*, 130–139.
- (9) Sun, S.; Li, Q.; Zhao, N.; Jiang, J.; Zhang, K.; Hou, J.; Wang, X.; Liu, G. Preparation of highly interconnected porous poly (ϵ -caprolactone)/poly (lactic acid) scaffolds via supercritical foaming. *Polym. Adv. Technol.* **2018**, *29*, 3065–3074.
- (10) Kuang, T.; Chen, F.; Chang, L.; Zhao, Y.; Fu, D.; Gong, X.; Peng, X. Facile preparation of open-cellular porous poly (l-lactic acid) scaffold by supercritical carbon dioxide foaming for potential tissue engineering applications. *Chem. Eng. J.* **2017**, *307*, 1017–1025.
- (11) Duarte, A. R. C.; Mano, J. F.; Reis, R. L. Supercritical fluids in biomedical and tissue engineering applications: a review. *Int. Mater. Rev.* **2009**, *54*, 214–222.
- (12) Zhang, K.; Mohanty, A. K.; Misra, M. J. Fully biodegradable and biorenewable ternary blends from polylactide, poly (3-hydroxybutyrate-co-hydroxyvalerate) and poly (butylene succinate) with balanced properties. *ACS Appl. Mater. Interfaces* **2012**, *4*, 3091–3101.
- (13) Ding, W.; Chu, R. K.; Mark, L. H.; Park, C. B.; Sain, M. Non-isothermal crystallization behaviors of poly (lactic acid)/cellulose nanofiber composites in the presence of CO₂. *Eur. Polym. J.* **2015**, *71*, 231–247.
- (14) Nissilä, T.; Hietala, M.; Oksman, K. A method for preparing epoxy-cellulose nanofiber composites with an oriented structure. *Composites, Part A* **2019**, *125*, No. 105515.
- (15) Song, J.; Mi, J.; Zhou, H.; Wang, X.; Zhang, Y. Chain extension of poly (butylene adipate-co-terephthalate) and its microcellular foaming behaviors. *Polym. Degrad. Stab.* **2018**, *157*, 143–152.
- (16) Barmouz, M.; Behraves, A. H. Statistical and experimental investigation on low density microcellular foaming of PLA-TPU/cellulose nano-fiber bio-nanocomposites. *Polym. Test.* **2017**, *61*, 300–313.
- (17) Soeta, H.; Fujisawa, S.; Saito, T.; Isogai, A. Controlling miscibility of the interphase in polymer-grafted nanocellulose/cellulose triacetate nanocomposites. *ACS Omega* **2020**, *5*, 23755–23761.
- (18) Ratheesh, G.; Venugopal, J. R.; Chinappan, A.; Ezhilarasu, H.; Sadiq, A.; Ramakrishna, S. 3D fabrication of polymeric scaffolds for regenerative therapy. *ACS Biomater. Sci. Eng.* **2017**, *3*, 1175–1194.
- (19) Zhang, K.; Wang, Y.; Jiang, J.; Wang, X.; Hou, J.; Sun, S.; Li, Q. Fabrication of highly interconnected porous poly (ϵ -caprolactone) scaffolds with supercritical CO₂ foaming and polymer leaching. *J. Mater. Sci.* **2019**, *54*, 5112–5126.
- (20) Qiao, Y.; Li, Q.; Jalali, A.; Yang, J.; Wang, X.; Zhao, N.; Jiang, Y.; Wang, S.; Hou, J.; Jiang, J. In-situ microfibrillated Poly (ϵ -caprolactone)/Poly (lactic acid) composites with enhanced rheological properties, crystallization kinetics and foaming ability. *Composites, Part B* **2021**, *208*, No. 108594.
- (21) Li, Y.; Mi, J.; Fu, H.; Zhou, H.; Wang, X. Nanocellular foaming behaviors of chain-extended poly (lactic acid) induced by isothermal crystallization. *ACS Omega* **2019**, *4*, 12512–12523.
- (22) Marrazzo, C.; Di Maio, E.; Iannace, S.; Nicolais, L. Process-structure relationships in PCL foaming. *J. Cell. Plast.* **2008**, *44*, 37–52.
- (23) Lin, N.; Huang, J.; Dufresne, A. Preparation, properties and applications of polysaccharide nanocrystals in advanced functional nanomaterials: a review. *Nanoscale* **2012**, *4*, 3274–3294.
- (24) Yang, X.; Berglund, L. A. Structural and ecofriendly holocellulose materials from wood: microscale fibers and nanoscale fibrils. *Adv. Mater.* **2021**, *33*, No. 2001118.
- (25) Jiang, J.; Li, Z.; Yang, H.; Wang, X.; Li, Q.; Turng, L. S. Microcellular injection molding of polymers: a review of process know-how, emerging technologies, and future directions. *Curr. Opin. Chem. Eng.* **2021**, *33*, No. 100694.
- (26) Cui, X.; Honda, T.; Asoh, T.-A.; Uyama, H. Cellulose modified by citric acid reinforced polypropylene resin as fillers. *Carbohydr. Polym.* **2020**, *230*, No. 115662.
- (27) Espino-Pérez, E.; Bras, J.; Ducruet, V.; Guinault, A.; Dufresne, A.; Domenek, S. Influence of chemical surface modification of cellulose nanowhiskers on thermal, mechanical, and barrier properties of poly (lactide) based bionanocomposites. *Eur. Polym. J.* **2013**, *49*, 3144–3154.
- (28) Kriechbaum, K.; Munier, P.; Apostolopoulou-Kalkavoura, V.; Lavoine, N. Analysis of the porous architecture and properties of anisotropic nanocellulose foams: a novel approach to assess the quality of cellulose nanofibrils (CNFs). *ACS Sustainable Chem. Eng.* **2018**, *6*, 11959–11967.
- (29) Wang, Q.; Asoh, T. A.; Uyama, H. Ultralight Bacterial Cellulose/Polypropylene-graft-Maleic Anhydride Composite Cryogel for Efficient Oil/Water Separation. *Chem. Lett.* **2021**, *50*, 14–16.
- (30) Zhou, H.; Zhao, M.; Qu, Z.; Mi, J.; Wang, X.; Deng, Y. J. Thermal and rheological properties of poly (lactic acid)/low-density polyethylene blends and their supercritical CO₂ foaming behavior. *J. Polym. Environ.* **2018**, *26*, 3564–3573.
- (31) Ray, S. S.; Okamoto, M. J. M. Biodegradable polylactide and its nanocomposites: opening a new dimension for plastics and composites. *Macromol. Rapid Commun.* **2003**, *24*, 815–840.
- (32) Jiang, C.; Han, S.; Chen, S.; Zhou, H.; Wang, X. The role of PTFE in-situ fibrillation on PET microcellular foaming. *Polymer* **2021**, *212*, No. 123171.
- (33) Li, L.; Li, W.; Geng, L.; Chen, B.; Mi, H.; Hong, K.; Peng, X.; Kuang, T. Formation of stretched fibrils and nanohybrid shish-kebabs in isotactic polypropylene-based nanocomposites by application of a dynamic oscillatory shear. *Chem. Eng. J.* **2018**, *348*, 546–556.

- (34) Song, Y.; Tashiro, K.; Xu, D.; Liu, J.; Bin, Y. Crystallization behavior of poly (lactic acid)/microfibrillated cellulose composite. *Polymer* **2013**, *54*, 3417–3425.
- (35) Nassiopoulos, E.; Njuguna, J. Thermo-mechanical performance of poly (lactic acid)/flax fibre-reinforced biocomposites. *Mater. Des.* **2015**, *66*, 473–485.
- (36) Cannillo, V.; Chiellini, F.; Fabbri, P.; Sola, A. Production of Bioglass 45S5–Polycaprolactone composite scaffolds via salt-leaching. *Compos. Struct.* **2010**, *92*, 1823–1832.
- (37) Leung, S. N.; Wong, A.; Guo, Q.; Park, C. B.; Zong, J. H. Change in the critical nucleation radius and its impact on cell stability during polymeric foaming processes. *Chem. Eng. J.* **2009**, *64*, 4899–4907.
- (38) Castaño, M.; Martínez-Campos, E.; Pintado-Sierra, M.; García, C.; Reinecke, H.; Gallardo, A.; Rodríguez-Hernández, J.; Elvira, C. Combining breath figures and supercritical fluids to obtain porous polymer scaffolds. *ACS Omega* **2018**, *3*, 12593–12599.
- (39) Wang, L.; Ishihara, S.; Hikima, Y.; Ohshima, M.; Sekiguchi, T.; Sato, A.; Yano, H. Unprecedented development of ultrahigh expansion injection-molded polypropylene foams by introducing hydrophobic-modified cellulose nanofibers. *ACS Appl. Mater. Interfaces* **2017**, *9*, 9250–9254.
- (40) Lavoine, N.; Bergström, L. Nanocellulose-based foams and aerogels: Processing, properties, and applications. *J. Mater. Chem. A* **2017**, *5*, 16105–16117.
- (41) Lee, J. W.; Park, C. B. Use of Nitrogen as a Blowing Agent for the Production of Fine-Celled High-Density Polyethylene Foams. *Macromol. Mater. Eng.* **2006**, *291*, 1233–1244.
- (42) Yang, Q.; Chen, L.; Shen, X.; Tan, Z. Physics, Preparation of polycaprolactone tissue engineering scaffolds by improved solvent casting/particulate leaching method. *J. Macromol. Sci., Part B: Phys.* **2006**, *45*, 1171–1181.
- (43) Guo, H.; Jiang, J.; Li, Z.; Jin, Z.; Hou, J.; Wang, X.; Li, Q. Solid-State Supercritical CO₂ Foaming of PCL/PLGA Blends: Cell Opening and Compression Behavior. *J. Polym. Environ.* **2020**, *28*, 1880–1892.